Signature of a Z_2 vortex in the dynamical correlations of the triangular-lattice Heisenberg antiferromagnet

Tsuyoshi Okubo*, Hikaru Kawamura

Department of Earth and Space Science, Faculty of Science, Osaka University, Toyonaka 560-0043, Japan

Dynamical properties of the classical Heisenberg antiferromagnet on the triangular lattice are investigated by means of a spin-dynamics simulation and an analytical calculation. While the model was suggested to exhibit a topological transition driven by the Z_2-vortex binding-unbinding, weakness of the associated thermodynamic singularity has made it difficult to observe the evidence of the Z_2 vortex experimentally so far, only some indirect support. Here, we show that the signature of the Z_2-vortex excitation and the vortex-induced topological transition can be captured from the dynamical spin correlations. In particular, the dynamical spin structure factor exhibits a characteristic central peak around the Z_2-vortex transition, and this central peak will be a fingerprint of the Z_2-vortex excitation.

KEYWORDS: frustration, triangular lattice, dynamical spin structure factor, Z_2 vortex, spin-dynamics simulation, topological transition

1. Introduction

Recently, geometrically frustrated magnets have attracted much interest because of their unconventional ordering behaviors, including the possible quantum spin-liquid state[1] and the novel ordered states like chiral ordered state,[2,3] spin nematic or multipolar state,[4,5] spin-gel state[6] *etc*. Such novel ordered states as well as the associated phase transitions are often borne by novel excitations inherent to frustrated systems. One typical example might be a Z_2 vortex, stabilized in a class of two-dimensional (2D) Heisenberg magnet with the locally noncollinear spin order,[7] *e.g.*, the frustrated Heisenberg antiferromagnet (AF) on the triangular lattice (Fig.1).

Indeed, the AF Heisenberg model on the 2D triangular lattice is a typical example of geometrically frustrated magnets and has been extensively studied as the standard model of frustrated systems. In recent experiments on the triangular-lattice Heisenberg AFs S=3/2 $NaCrO_2$,[8–11] S=1 $NiGa_2S_4$[12–18] and S=1/2 organic compounds, κ-$(BEDT\text{-}TTF)_2Cu_2(CN)_3$[19–21] or $EtMe_3Sb[Pd(dmit)_2]_2$,[22,23] a spin-liquid like behavior without the standard magnetic long-range order was observed, while all of these compounds exhibit a weak but clear transition-like anomaly at a finite temperature. As a possible explanation of the observed experimental behavior, ref. 6 suggested a Z_2 vortex as a key ingredient. Experimentally observed weak anomaly was then ascribed to the Z_2-vortex driven topological transition, while the observed low-temperature state to the "spin-gel" state where the spin correlation length is kept finite while the ergodicity is broken topologically.[6,24]

If one considers the simplest case of the classical AF Heisenberg model with the nearest-neighbor AF coupling, the ground state is the so-called 120-degrees structure. It was demonstrated by Kawamura and Miyashita that the model sustained a topologically stable point defect characterized by a two-valued topological quantum number, a Z_2 vortex[7] (Fig.1). They suggested that, though the AF spin correlation length remains finite at any finite temperature $T > 0$, a thermodynamic phase transition driven by the binding-unbinding of the Z_2 vortices occurred at a finite temperature.

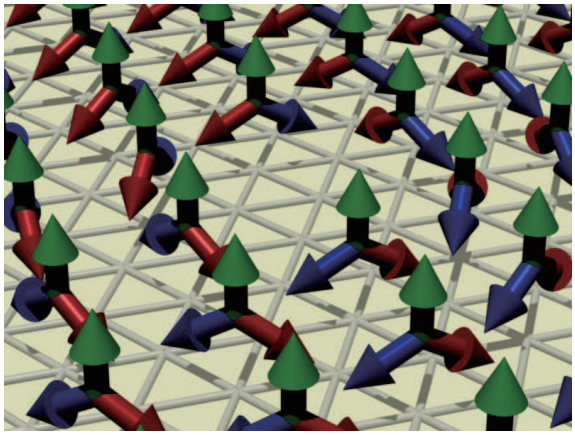

Fig. 1. (Color online) Illustration of a Z_2 vortex formed by the local 120-degrees structure realized in the antiferromagnetic Heisenberg model on the triangular lattice.

The remarkable feature of the Z_2-vortex transition might be the decoupling of the two length scales, a spin-wave (SW) correlation length ξ_{sw} and a vortex correlation length ξ_v, the latter corresponding to the mean separation of free Z_2 vortices.[6] At the Z_2-vortex transition temperature $T = T_v$, the vortex correlation length ξ_v diverges, while the spinwave correlation length ξ_{sw} is kept finite (Fig.2). In the high-temperature regime $T \gg T_v$ where $\xi_v \ll \xi_{sw}$, the standard spin correlation length ξ is dominated by vortices $\xi \simeq \xi_v$, while, in the low-temperature regime, ξ is dominated by spinwaves $\xi \simeq \xi_{sw}$. Note that, because of the finiteness of ξ_{sw}, the full spin correlation length is kept finite even at $T < T_v$. The relative importance of vortices and spinwaves is interchanged around a crossover tempera-

*E-mail address: okubo@spin.ess.sci.osaka-u.ac.jp

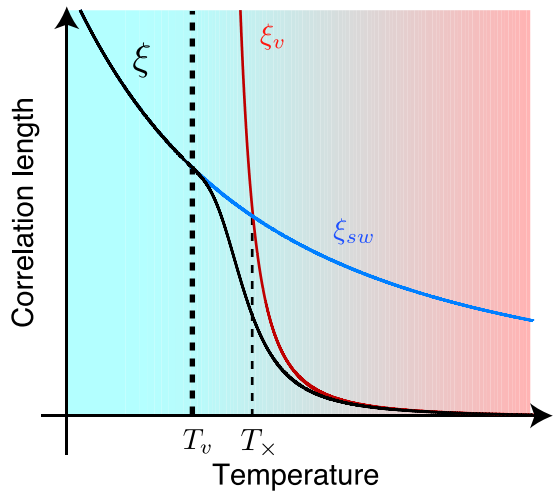

Fig. 2. (Color online) Schematic picture of the decoupling between vortices and spinwaves, each characterized by the associated correlation length, ξ_v and ξ_{sw}. At the Z_2-vortex transition temperature T_v, the vortex correlation-length ξ_v diverges, while the spinwave correlation length ξ_{sw} is kept finite. The behavior of the full spin correlation length ξ is also shown. In the low-temperature spin-gel state, the spin correlation is dominated by spinwave excitations, whereas, in the high-temperature phase, the spin correlation is dominated by vortex excitations. There exists a crossover temperature $T_\times (> T_v)$ at which the relative importance of vortices and spinwaves are interchanged. T_v and $T_\times$ were estimated by the recent Monte Carlo simulation to be $T_v = 0.285 \pm 0.005$ and $T_\times \simeq 0.294$ (ref. 6).

ture $T_\times (> T_v)$ at which $\xi_v \simeq \xi_{sw}$ (Fig.2). Such a decoupling behaviour is in sharp contrast to the behavior in other vortex-driven transitions, *i.e.*, the Kosterlitz-Thouless (KT) transition of the 2D XY model, where there exists only one length scale and the spin correlation length stays infinite throughout the low temperature phase.[25,26]

According to a recent theoretical analysis,[6] the diverging behavior of ξ_v is given by

$$\xi_v \sim \exp\left[\left(\frac{A}{T - T_v}\right)^{\alpha}\right], \quad T > T_v, \tag{1}$$

where $\alpha < 1$. The usual thermodynamic macroscopic observables such as the specific heat or the magnetic susceptibility show only a week essential singularity at T_v, which makes the direct experimental observation of the Z_2-vortex transition rather difficult. So far, only an indirect experimental support was reported.[8,16,17]

In this paper, we concentrate on the *dynamical* properties of the model in search for the signature of a Z_2 vortex. Our numerical result indicates that the signature of a Z_2-vortex and a Z_2-vortex driven topological transition can be captured from the information of *dynamical* spin correlations, specifically from that of the dynamical spin structure factor, which can be measured by means of inelastic neutron scattering.

The rest of the paper is organized as follows. In Sec. 2, we describe the model and details of our spin-dynamics simulation. In Sec. 3, we present the result of our numerical simulation and analytical calculation, and discuss their relation to the Z_2-vortex excitation. In Sec. 4, we conclude with a summary and implications to experiments.

2. Model and Method

The model we consider is the classical Heisenberg AF on the two-dimensional triangular lattice, whose Hamiltonian is given by

$$\mathcal{H} = J \sum_{\langle i,j \rangle} \vec{S}_i \cdot \vec{S}_j, \tag{2}$$

where $J > 0$, and the sum is taken over all nearest-neighbor pairs. We perform here a spin-dynamics simulation of the model. The lattice is a $L \times L$ triangular lattice of a rhomboidal shape with periodic boundary conditions. The dynamics is assumed to obey the classical analogue of the Bloch equation,

$$\hbar \frac{d\vec{S}_i}{dt} = J \left(\sum_{\delta} \vec{S}_\delta \right) \times \vec{S}_i, \tag{3}$$

where the sum is taken over all nearest neighbours. Note that this dynamics conserves the total energy as well as the total uniform magnetization $\vec{M} = \sum_i \vec{S}_i$. The temperature effect is taken into account via initial spin configurations, which are generated from the standard equilibrium Monte Carlo (MC) simulation at the temperature T. Dynamical observables are calculated by averaging over $500 - 1000$ independent spin-dynamics simulations starting from different initial configurations prepared by equilibrium MC runs.

In order to prepare initial spin configurations for our spin-dynamics simulations, we generate equilibrium spin configurations at a given temperature T by first performing a hybrid Monte Carlo simulation which consists of the heat-bath updating and the over-relaxation updating. One hybrid MC step (MCS) consists of one heat-bath and ten over-relaxation sweeps. At each temperature, we generate such equilibrium spin configurations, which are taken from our MC run every 10^3 MCS after discarding 10^5 MCS for equilibration.

In our spin-dynamics simulation, we employ a recently developed second-order decomposition method to solve equation (3) numerically.[27,28] We set a time step $\delta t = 0.01\hbar J^{-1}$, and the integration of equation (3) is carried out to t_{max}, typically of the order of $t_{max} = 800\hbar J^{-1}$. We checked the accuracy of our simulation by comparing the obtained data at several temperatures with those obtained with a finer time step of $\delta t = 0.001\hbar J^{-1}$, and with those obtained by using the fourth-order Runge-Kutta method with a time step of $\delta t = 0.01\hbar J^{-1}$.

The dynamical spin structure factor is defined by

$$S(\boldsymbol{q}, \omega) \equiv \int d\boldsymbol{r} \int dt \left\langle \vec{S}_{\boldsymbol{0}}(0) \cdot \vec{S}_{\boldsymbol{r}}(t) \right\rangle \exp[-i(\omega t + \boldsymbol{q} \cdot \boldsymbol{r})]. \tag{4}$$

where ω is the angular frequency, $\boldsymbol{q}$ is the wavevector, and $\langle \cdots \rangle$ denotes a thermal average.

The dynamical spin structure factor is calculated via

the formula,

$$\tilde{S}(\boldsymbol{q},\omega) = \left\langle |\vec{S}_{\boldsymbol{q}}(\omega)|^2 \right\rangle, \tag{5}$$

where $\langle \cdots \rangle$ represents an average over initial spin configurations, and $\vec{S}_{\boldsymbol{q}}(\omega)$ is the space-time Fourier transform of the spin variable given by

$$\vec{S}_{\boldsymbol{q}}(\omega) \equiv \int dt \sum_i \vec{S}_i(t) \exp[-i(\boldsymbol{q}\cdot\boldsymbol{r}_i + \omega t)]. \tag{6}$$

In order to decrease statistical errors, the dynamical spin structure factor is symmetrized as

$$S(\boldsymbol{q},\omega) \equiv \frac{\tilde{S}(\boldsymbol{q},\omega) + \tilde{S}(\boldsymbol{q},-\omega)}{2}. \tag{7}$$

The central component of $S(\boldsymbol{q},\omega)$ is often subject to pronounced finite-size effect. We have checked the system-size dependence of $S(\boldsymbol{q},\omega)$ by comparing those of $L = 192, 384, 768$ at each temperature for the triangular case, to confirm that the data shown here are close enough to the bulk ones.

3. Results

In Fig.3a, we show the frequency dependence of the dynamical spin structure factor $S(\boldsymbol{q},\omega)$ at a wavevector $\boldsymbol{q} = (4\pi/3{+}4\pi/192, 0)$, slightly off the K-point. Note that the perfect 120-degrees structure yields the magnetic Bragg peak at the K-point, $\boldsymbol{q}_K = (4\pi/3, 0)$. The temperature range studied is below around the specific-heat peak temperature $T_{peak} \simeq 0.32$, including both above and below $T_v \simeq 0.285$. As can be seen from the figure, at a temperature $T = 0.280$ slightly below T_v, $S(\boldsymbol{q},\omega)$ exhibits only two side peaks corresponding to spinwave excitations. On increasing the temperature, in addition to the spinwave peaks, a *central peak* centered at $\omega = 0$ appears and grows. The central peak and the spinwave peaks coexist in the range $0.290 \lesssim T \lesssim 0.305$, whereas, at higher temperatures, these peaks are merged into a single broad peak at $\omega = 0$ with spinwave shoulders remaining at finite ω. At $T = 0.305$, the intensity of the central peak is about 1% of that at the K point. The width of the central peak is of the same amount as that of the spinwave peak, showing no pronounced tendency to sharpen toward $T \to T_v$. Note that the onset of the central component in $S(\boldsymbol{q},\omega)$ is fully correlated to the vortex transition at $T = T_v \simeq 0.285$. This correspondence suggests that the observed central peak might be originated from the contribution of free Z_2 vortices.

In order to further clarify the situation, we also compute $S(\boldsymbol{q},\omega)$ for the unfrustrated 2D Heisenberg AF on a square lattice, a model which does not bear a Z_2 vortex. The result is shown in Fig.3b for the temperatures below around the specific-heat peak temperature $T_{peak} \simeq 0.68$. In sharp contrast to the triangular case, no central peak is observed in the low-temperature regime where spinwave peaks exist. This absence of the central peak coexisting with the spinwave peaks supports the view that the central peak observed in the triangular case is due to free Z_2 vortices.

We next perform a simplified theoretical analysis of the dynamical spin structure factor based on the spinwave-vortex decoupling picture. We start with a simple assumption of the factorization of the dynamical spin-spin correlation function $C(\boldsymbol{r},t)$ into the vortex part and the spinwave part

$$C(\boldsymbol{r},t) \equiv \left\langle \vec{S}_{\boldsymbol{0}}(0)\cdot\vec{S}_{\boldsymbol{r}}(t) \right\rangle \simeq C_v(\boldsymbol{r},t) C_{sw}(\boldsymbol{r},t), \tag{8}$$

where $C_{sw}(\boldsymbol{r},t)$ is a dynamical spin correlation function due to the spinwave excitations and $C_v(\boldsymbol{r},t)$ is the one due to the Z_2-vortex excitations. We assume that the space Fourier transform of $C_{sw}(\boldsymbol{r},t)$ is governed by the spinwave mode with a dispersion $\omega_{sw}(\boldsymbol{q})$ and with a damping $\tau_{sw}(\boldsymbol{q})$ as

$$C_{sw}(\boldsymbol{q},t) = S_{sw}(\boldsymbol{q}) \exp[-t/\tau_{sw}(\boldsymbol{q}) \pm i\omega_{sw}(\boldsymbol{q})t], \tag{9}$$

where $S_{sw}(\boldsymbol{q})$ is the static spin structure factor due to spinwaves. We also assume that the corresponding vortex-part is given by a simple exponential form as

$$C_v(\boldsymbol{q},t) = S_v(\boldsymbol{q}) \exp[-t/\tau_v], \tag{10}$$

where $S_v(\boldsymbol{q})$ is the static spin structure factor due to vortices, and τ_v is assumed to be $\boldsymbol{q}$-independent. From eqs. (8)-(10), $S(\boldsymbol{q},\omega)$ is obtained as the convolution of the spinwave part and the vortex part as

$$S(\boldsymbol{q},\omega) = \int d\boldsymbol{q}' \frac{2\tau(\boldsymbol{q}-\boldsymbol{q}')S_{sw}(\boldsymbol{q}-\boldsymbol{q}')S_v(\boldsymbol{q}')}{1+[\tau(\boldsymbol{q}-\boldsymbol{q}')]^2[\omega \pm \omega_{sw}(\boldsymbol{q}-\boldsymbol{q}')]^2}, \tag{11}$$

where the reduced correlation time is given by $1/\tau(\boldsymbol{q}) \equiv 1/\tau_{sw}(\boldsymbol{q}) + 1/\tau_v$. The peak of $S_{sw}(\boldsymbol{q})$ is located at the K point, while $S_v(\boldsymbol{q})$ is expected to be peaked at $\boldsymbol{q} = 0$. Thus, $S(\boldsymbol{q},\omega)$ typically exhibit two peaks, one at $\omega = \omega_{sw}(\boldsymbol{q})$ and the other at $\omega = \omega_{sw}(\boldsymbol{q}_K)$. Since $\omega_{sw}(\boldsymbol{q}_K) = 0$, the latter corresponds to the central peak. At the Z_2-vortex transition $T = T_v$, the vortex correlation length ξ_v diverges, and in the low temperature spin-gel state, $S_v(\boldsymbol{q}) \propto \delta(\boldsymbol{q})$. Thus, in the spin-gel state below T_v, $S(\boldsymbol{q},\omega)$ is determined solely by spinwaves without a central-peak structure.

In Fig.3c, we show a typical form of $S(\boldsymbol{q},\omega)$ above T_v calculated from eq. (11) under several assumptions given in the caption of Fig.3. As can be seen from the figure, the observed shape of the dynamical spin structure factor is well reproduced by (11), at least qualitatively, as long as $\tau(\boldsymbol{q})$ is taken to be moderately small. This observation gives further support to the view that the central peak of $S(\boldsymbol{q},\omega)$ is originated from free Z_2 vortices.

Another explanation of the central peak of $S(\boldsymbol{q},\omega)$ was suggested by Mertens *et al* in terms of the KT vortices of the 2D XY model.[29] Based on a dilute vortex-gas picture, these authors estimated the free-vortex contribution to $S(\boldsymbol{q},\omega)$ in the form of squared Lorenzian.[29] The data of several spin-dynamics simulations on the 2D XY model were interpreted in terms of this theory.[29–31] In our observation, however, the motion of Z_2 vortices are incompatible with such a dilute gas picture. The Z_2 vortices of the present model behave *diffusively* so that the root-mean-squared displacement of the free vortices

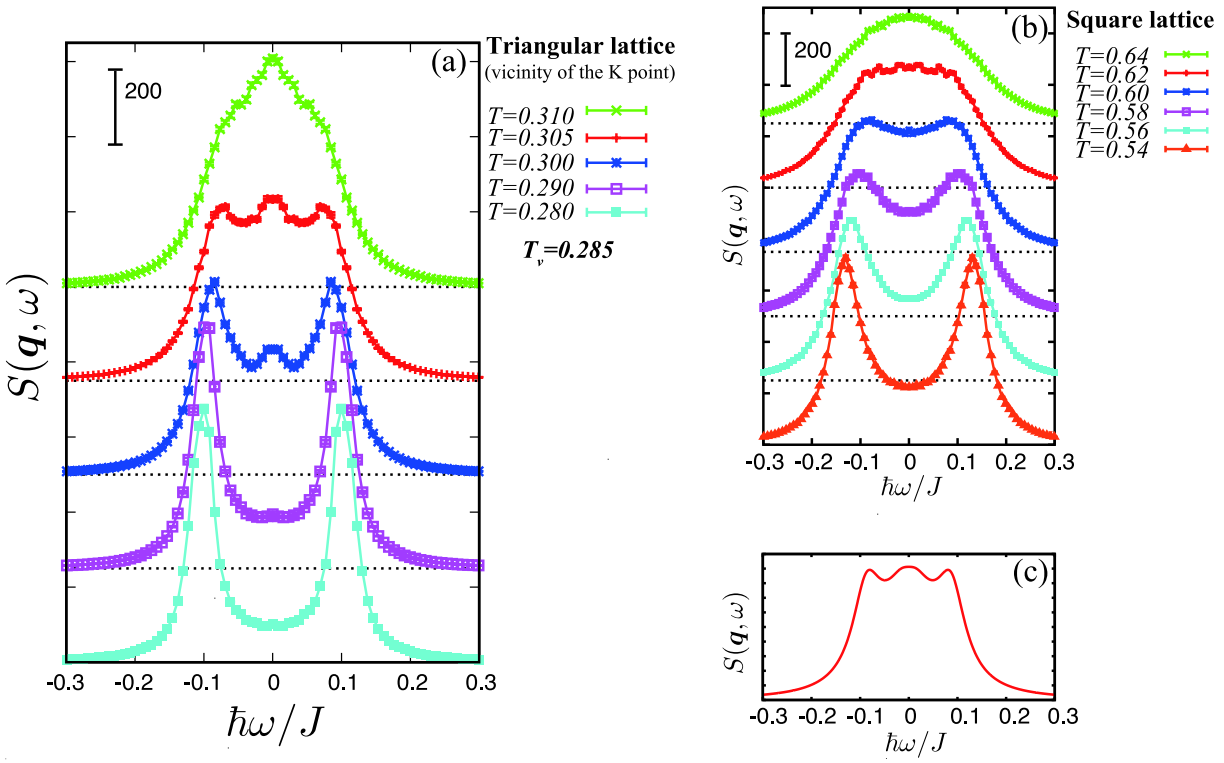

Fig. 3. (Color online) (a) The frequency dependence of the dynamical structure factor of the triangular-lattice Heisenberg antiferromagnet at a wavevecotr $\boldsymbol{q} = (4\pi/3 + 4\pi/192, 0)$ near the K point for the temperatures below around the specific-heat maximum temperature $T < T_{peak} \simeq 0.32$ including both below and above $T_v \simeq 0.285$. The lattice size is $L = 768$. For better visualization, baselines of the data at different temperatures are shifted vertically (dotted lines). (b) The frequency dependence of the dynamical structure factor of the square-lattice Heisenberg antiferromagnet at a wavevecotr $\boldsymbol{q} = (\pi - 2\pi/128, \pi - 2\pi/128)$ for the temperatures below around the specific-heat maximum temperature $T < T_{peak} \simeq 0.68$. The lattice size is $L = 256$. (c) A typical pattern of the dynamical structure factor calculated from eq. (11) by assuming Lorenzian forms for $S_{sw}(\boldsymbol{q})$ and $S_v(\boldsymbol{q})$, $S_{sw}(\boldsymbol{q}) \propto 1/[1+\xi_{sw}^2(\boldsymbol{q}-\boldsymbol{q}_K)^2]$ and $S_v(\boldsymbol{q}) \propto 1/[1+\xi_v^2\boldsymbol{q}^2]$, with a linear dispersion relation, $\omega_{sw}(\boldsymbol{q}) = v_{sw}|\boldsymbol{q}-\boldsymbol{q}_K|$ and neglecting the $\boldsymbol{q}$-dependence of $\tau(\boldsymbol{q})$. The parameters in eq. (11) are $\xi_v = 250, \xi_{sw} = 150$, $\boldsymbol{q} = (4\pi/3 + 4\pi/192, 0)$, $\tau(\boldsymbol{q}) = 40$ and $v_{sw} = 1.36$. The central peak arises when τ is moderately small, $1/\omega_{sw}(\boldsymbol{q}) \lesssim \tau \lesssim \xi_{sw}/v_{sw}$.

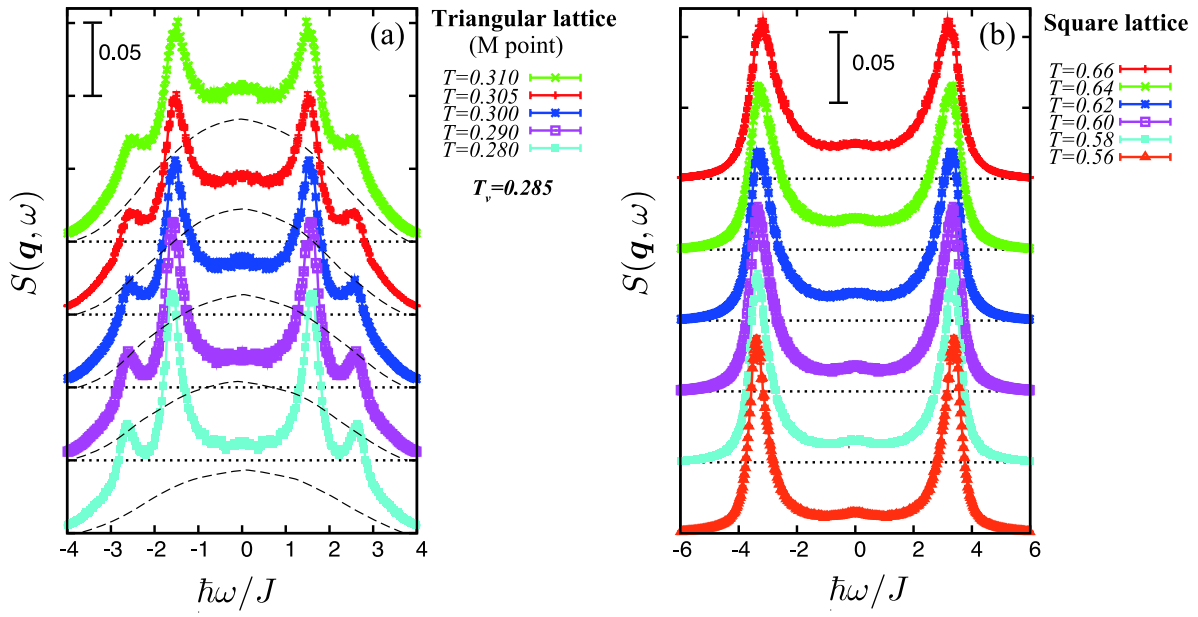

Fig. 4. (Color online) (a) The frequency dependence of the dynamical spin structure factor of the triangular-lattice Heisenberg antiferromagnet at a wavevecotr $\boldsymbol{q} = (0, 2\pi/\sqrt{3})$ corresponding to the M point for the temperatures as in Fig.3a. The lattice size is $L = 768$. For better visualization, baselines of the data at different temperatures are shifted vertically (dotted lines). As a guide to the eye, the central component referred in the main text is indicated by the dashed lines. (b) The frequency dependence of the dynamical structure factor of the square-lattice Heisenberg antiferromagnet at a wavevecotr $\boldsymbol{q} = (0, \pi)$ for the temperatures as in Fig.3b. The lattice size is $L = 256$.

is proportional to the square root of the elapsed time t as $\sqrt{\langle \delta r^2(t) \rangle} \propto \sqrt{t}$. Hence, the origin of the central peak observed in the present model probably differs from the one proposed by Mertens *et al* for the KT vortices.

The central peak of $S(\boldsymbol{q}, \omega)$ is not limited to the vicinity of the K point. A broad central component also appears even at wavevectors away from the K point, though its intensity is significantly reduced and its width is much broadened. In Fig.4a, we show the ω-dependence of $S(\boldsymbol{q}, \omega)$ at the M point, $\boldsymbol{q} = \boldsymbol{q}_M = (0, 2\pi/\sqrt{3})$. In addition to the spinwave side peaks, a broad but distinct central component centered at $\omega = 0$ exists. Note that the width of the central component is larger than that near the K point by an order of magnitude, while its intensity is weaker than that near the K point by a factor of 10^{-3}. The intensity of the central component tends to be decreased with decreasing the temperature as in the vicinity of the K point.

For comparison, we show in Fig.4b $S(\boldsymbol{q}, \omega)$ of the square-lattice Heisenberg AF at the zone boundary, $\boldsymbol{q} = (0, \pi)$. The computed $S(\boldsymbol{q}, \omega)$ hardly exhibits a central peak. Though a faint central component is discernible, its intensity is significantly weaker than that of the spinwave peak, and the difference from the triangular case shown in Fig.4a is distinct.

We then ascribe the origin of the broad central component observed away from the K point to the contribution of the Z_2 vortex-pair excitations. Near the K point, the central peak of $S(\boldsymbol{q}, \omega)$ predominantly probes the dynamics of free Z_2 vortices, while, as one moves away from the K point, the central component tends to probe the dynamics of more tightly bound Z_2-vortex pairs. Our observation that the width of the central component becomes significantly larger when one moves away from the K point (see Fig.3a and Fig.4a) means that the time scale of underlying dynamics becomes considerably faster. This seems fully consistent with our identification above, since tightly bound pairs tend to yield faster dynamics associated with pair annihilation and creation than that of free vortices. Another feature to be noticed is that, at the $\boldsymbol{q}$ points away from the K point, *e.g.*, at the M point, the central component of $S(\boldsymbol{q}, \omega)$ tends to persist even at $T < T_v$. This observation also supports our interpretation above, since the vortex pair can stably exist even below T_v unlike the free vortex.

In order to illustrate the broad central component observed for a wide range of wavevecotrs, we show in Fig.5a the intensity map of $S(\boldsymbol{q}, \omega)$ in the entire $\boldsymbol{q}$-plane at $\hbar\omega/J \simeq 1$ at a temperature slightly above T_v, $T = 0.31$. The effect of the central components is observed as the intensities near the Brillouin zone boundaries, which appear in addition to bright ring-like intensities surrounding the K points corresponding to spinwave excitations. We note that such intensities near the zone boundaries cannot be seen in the corresponding intensity map of the square-lattice Heisenberg AF shown in Fig.5b.

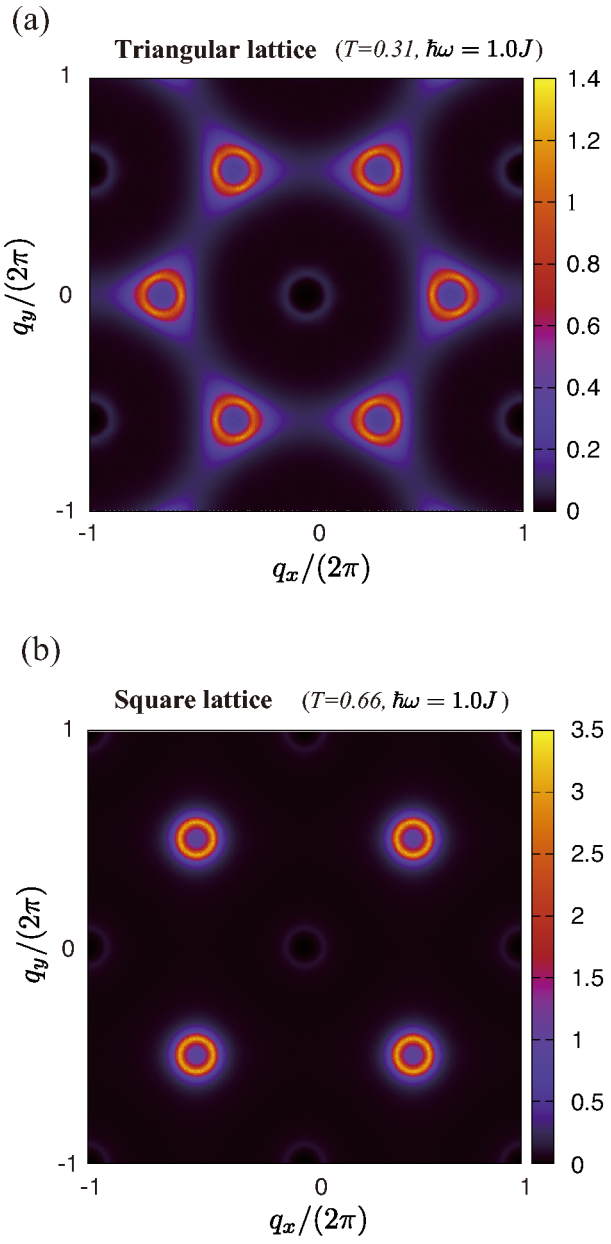

Fig. 5. (Color online) (a),(b) the intensity maps of the dynamical spin structure factor in the wavevecotr space with $\hbar\omega = J$, for the case of the triangular-lattice Heisenberg antiferromagnet with $L = 192$ at a temperature $T = 0.31$ (a), and for the case of the square-lattice Heisenberg antiferromagnet with $L = 256$ at a temperature $T = 0.66$ (b).

4. Summary and Discussion

From all these observations, we conclude that the central peak of the dynamical spin structure factor $S(\boldsymbol{q}, \omega)$ is originated from the Z_2-vortex excitation. The bases of our conclusion can be summarized as: i) Near the K point, the central peak appears only at $T > T_v$, increasing its intensity with increasing the temperature; ii) the central peak does not appear in the unfrustrated square-lattice Heisenberg AF, a model which does not sustain the Z_2 vortex; and iii) the central-peak structure similar to the one observed in our simulations can be reproduced by a simplified theoretical model based on the spinwave-vortex decoupling picture.

In contrast to the information of the standard spin correlation length ξ, which is obtainable via the elastic neutron scattering measurements, the information of the vortex correlation length ξ_v, that is the length scale

diverging at the vortex-transition point $T = T_v$, is hard to obtain. In principle, however, appropriate information about the central peak enables one to deduce ξ_v. On the basis of (11) together with the Lorenzian forms of $S_{sw}(\boldsymbol{q})$ and $S_v(\boldsymbol{q})$, the ratio of the central-peak intensity $I_c(\boldsymbol{q})$ to the spinwave one $I_{sw}(\boldsymbol{q})$ near the K point at $\boldsymbol{q} = \boldsymbol{q}_K + \delta\boldsymbol{q}$ is approximately obtained as $I_c/I_{sw} \sim \xi_{sw}/\xi_v$. By combining it with the information of the standard spin correlation length $\xi \sim \xi_{sw}\xi_v/(\xi_{sw} + \xi_v)$, we can estimate ξ_v together with ξ_{sw}.

Experimentally, the dynamical spin structure factor can be measured via inelastic neutron scattering. As mentioned, candidate triangular-lattice AFs possessing a Z_2 vortex excitation might be $NaCrO_2$, $NiGa_2S_4$ and organic compounds like κ-$(BEDT\text{-}TTF)_2Cu_2(CN)_3$ or $EtMe_3Sb[Pd(dmit)_2]_2$. Unfortunately, the organic compounds are not suited to neutrons so that neutron-scattering measurements seem unrealistic for these materials at the present stage. Then, promising candidate materials for the Z_2-vortex detection might be $NaCrO_2$ and $NiGa_2S_4$. These materials exhibit a transition-like anomaly at $T \simeq 30$K ($NaCrO_2$) and $T \simeq 8.5$K ($NiGa_2S_4$), slightly below the specific-heat peak temperature. Often, only powder samples are available for these materials. Under such circumstances, we also compute the angle-averaged dynamical spin structure factor $S(|\boldsymbol{q}|, \omega)$ to examine how $S(|\boldsymbol{q}|, \omega)$ looks like for powder samples, and the result is shown in Fig.6a and 6b for both cases of the $|\boldsymbol{q}|$-value close to $|\boldsymbol{q}| \simeq |\boldsymbol{q}_K|$ (a), and $|\boldsymbol{q}| \simeq |\boldsymbol{q}_M|$ (b). In both cases, the central peak is clearly observable together with the spinwave peaks. Thus, inelastic neutron scattering experiments for powder samples would be sufficient for observing the signature of a Z_2 vortex and a Z_2-vortex driven topological transition. This is a nice aspect for practical purpose, since one can expect the intensity gain for powder measurements.

Inelastic neutron-scattering measurements as suggested here might provide a useful information in understanding the spin-liquid-like behavior and the transition-like anomaly observed in triangular-lattice Heisenberg AFs $NaCrO_2$ and $NiGa_2S_4$, and the nature of novel excitations in geometrically frustrated magnets in general.

Acknowledgements

The authors would like to acknowledge S. Nakatsuji, M. Hagiwara, Y. Nambu and H. Yamaguchi for useful discussion. This work is supported by Grand-in-Aid for scientific Research on Priority Areas "Novel State of Matter Induced by Frustration" (19052006). We thank the Supercomputer Center, Institute for Solid State Physics, University of Tokyo for providing us with the CPU time.

1) P.W. Anderson: Mater. Res. Bull. **8** (1973) 153.
2) S. Miyashita, and H. Shiba: J. Phys. Soc. Jpn. **53** (1984) 1145 .
3) S. Onoda, and N. Nagaosa: Phys. Rev. Lett. **99** (2007) 027206.
4) H. Tsunetsugu, and M. Arikawa: J. Phys. Soc. Jpn. **75** (2006) 083701.
5) M.E. Zhitomirsky: Phys. Rev. B **78** (2008) 094423.
6) H. Kawamura, A.Yamamoto, and T. Okubo: J. Phys. Soc. Jpn. **79** (2010) 023701.
7) H. Kawamura, and S. Miyashita: J. Phys. Soc. Jpn. **53** (1984) 4138.
8) A. Olariu, P. Mendels, F. Bert, B.G. Ueland, P. Schiffer, R.F. Berger, and R.J. Cava: Phys. Rev. Lett. **97** (2006) 167203.
9) D. Hsieh, D. Qian, R.F. Berger, R.J. Cava, J.W. Lynn, Q. Huang, and M.Z. Hasan: Physica. B **403** (2008) 1341.
10) D. Hsieh, D.Qian, R.F. Berger, R.J. Cava, J.W. Lynn, Q. Huang, and M.Z. Hasan: J. Phys. Chem. Solids **69** (2008) 3174.
11) M. Hemmida, H.-A. Krug von Nidda, N. Büttgen, A. Loidl, L.K. Alexander, R. Nath, A.V. Mahajan, R.F. Berger, R.J. Cava, Y. Singh, and D.C. Johnston: Phys. Rev. B **80** (2009) 054406.
12) S. Nakatsuji, Y. Nambu, H. Tonomura, O. Sakai, S. Jonas, C. Broholm, H. Tsunetsugu, Y. Qiu, and Y. Maeno: Science **309** (2005) 1697.
13) Y. Nambu, S. Nakatsuji, and Y. Maeno: J. Phys. Soc. Jpn. **75** (2006) 043711.
14) H. Takeya, K. Ishida, K. Kitagawa, Y. Ihara, K. Onuma, Y. Maeno, Y. Nambu, S. Nakatsuji, D.E. MacLaughlin, A. Koda, and R. Kadono: Phys. Rev. B **77** (2008) 054429.
15) A. Yaouanc, P.D. de Réotier, Y. Chapuis, C. Marin, G. Lapertot, A. Cervellino, and A. Amato: Phys. Rev. B **77** (2008) 092403.
16) D.E. MacLaughlin, Y. Nambu, S. Nakatsuji, R.H. Heffner, L. Shu, O.O. Bernal, and K. Ishida: Phys. Rev. B **78** (2008) 220403(R).
17) H. Yamaguchi, S. Kimura, M. Hagiwara, Y. Nambu, S. Nakatsuji, Y. Maeno, and K. Kindo: Phys. Rev. B **78** (2008) 180404.
18) H. Yamaguchi, S. Kimura, M. Hagiwara, Y. Nambu, S. Nakatsuji, Y. Maeno, A. Matsuo, and K. Kindo: J. Phys. Soc. Jpn. **79** (2010) 054710.
19) Y. Shimizu, K. Miyagawa, K. Kanoda, M. Maesato, and G. Saito: Phys. Rev. Lett. **91** (2003) 107001.
20) S. Yamashita, Y. Nakazawa, M. Oguni, Y. Oshima, H. Nojiri, Y. Shimizu, K. Miyagawa, and K. Kanoda: Nature Physics **4** (2008) 459.
21) M. Yamashita, N. Nakata, Y. Kasahara, T. Sasaki, N. Yoneyama, N. Kobayashi, S. Fujimoto, T. Shibauchi, and Y. Matsuda: Nature Physics **5** (2009) 44.
22) M. Tamura, A. Nakao, and R. Kato: J. Phys. Soc. Jpn. **75** (2006) 093701.
23) T. Itou, A. Oyamada, S. Maegawa, M. Tamura, and R. Kato: Phys. Rev. B **77** (2008) 104413.
24) H. Kawamura, and A. Yamamoto: J. Phys. Soc. Jpn. **76** (2007) 073704.
25) J.M. Kosterliz, and D.J. Thouless: J. Phys. C: Solid State Phys. **6** (1973) 1181.
26) J.M. Kosterliz: J. Phys. C: Solid State Phys. **7** (1974) 1046 .
27) A. Krech, A. Bunker, and D.P. Landau: Comput. Phys. Commun. **111** (1998) 1.
28) S.-H. Tsai, M. Krech, and D.P. Landau: Braz. J. Phys. **34** (2004) 384.
29) F.G. Mertens, A.R. Bishop, G.M. Wysin, and C. Kawabata: Phys. Rev. B **39** (1989) 591.
30) H.G. Evertz, and D.P. Landau: Phys. Rev. B **54** (1996) 12302.
31) K. Nho, and D.P. Landau: Phys. Rev. B **66** (2002) 174403.

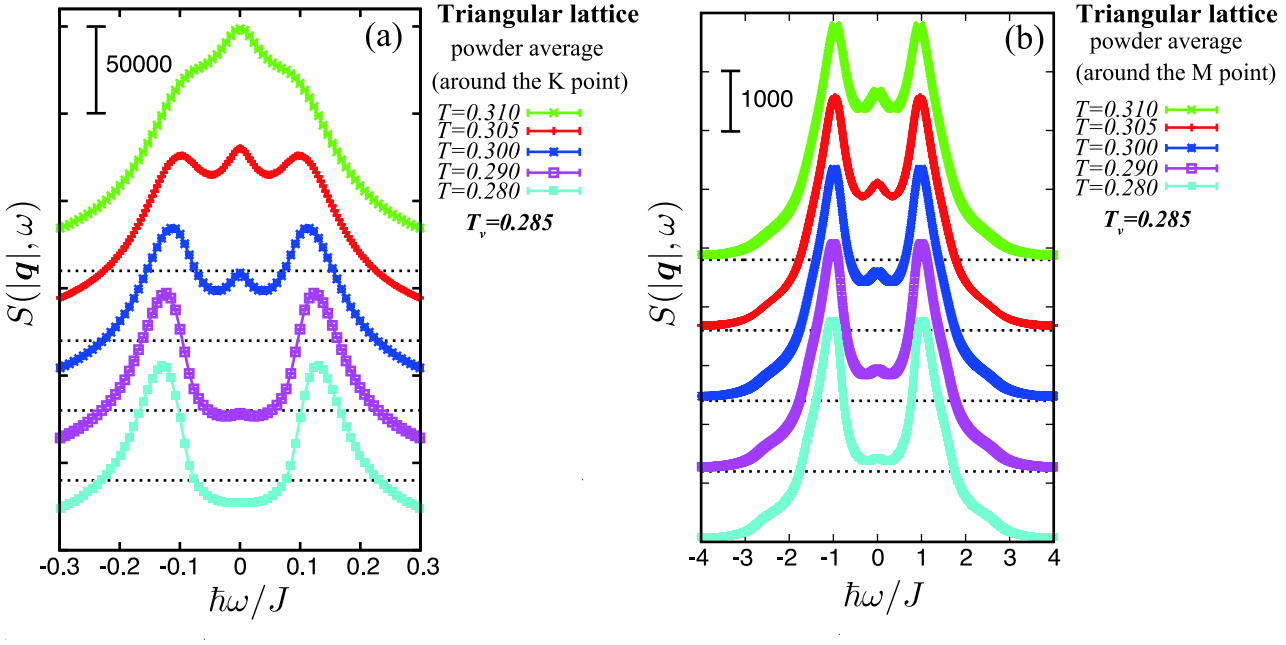

Fig. 6. (Color online) The frequency dependence of the angle-averaged dynamical spin structure factor of the triangular-lattice Heisenberg antiferromagnet for the temperatures as in Fig.3a and Fig.4a. The data should correspond to the neutron-scattering pattern obtained from powder samples. Panels (a) and (b) correspond to wavevectors satisfying $|\boldsymbol{q}_K| + 4\pi/192 \leq |\boldsymbol{q}| \leq |\boldsymbol{q}_K| + 6\pi/192$ (a), and $|\boldsymbol{q}_M| - 2\pi/384 \leq |\boldsymbol{q}| \leq |\boldsymbol{q}_M| + 2\pi/384$ (b).